Contrib Mineral Petrol (2003) 145: 578–584
DOI 10.1007/s00410-003-0467-9

ORIGINAL PAPER

**Elisabetta Brizi · Sabrina Nazzareni**
**Francesco Princivalle · Pier Francesco Zanazzi**

# Clinopyroxenes from mantle-related xenocrysts in alkaline basalts from Hannuoba (China): augite–pigeonite exsolutions and their thermal significance

Received: 27 November 2002 / Accepted: 20 March 2003 / Published online: 14 May 2003


**Abstract** Optically homogeneous augite xenocrysts, closely associated with spinel–peridotite nodules, occur in alkali basalts from Hannuoba (Hebei province, China). They were studied by electron and X-ray diffraction to define the occurrence and significance of pigeonite exsolution microtextures. Sub-calcic augite ($Wo_{34}$) exsolved into $En_{62-62}Fs_{25-21}Wo_{13-17}$ pigeonite and $En_{46-45}Fs_{14-14}Wo_{40-42}$ augite, as revealed by TEM through diffuse coarser (001) lamellae (100–300 Å) and only incipient (100) thinner ones ($< 70$ Å). $C2/c$ augite and $P2_1/c$ pigeonite lattices, measured by CCD-XRD, relate through $a$(Aug)≅$a$(Pgt), $b$(Aug)≅$b$(Pgt), $c$(Aug) ≠ $c$(Pgt) [5.278(1) vs 5.189(1)Å] and $\beta$(Aug) ≠ $\beta$(Pgt) [106.55(1) vs 108.55(2)°]. Cell and site volumes strongly support the hypothesis that the augite xenocrysts crystallised at mantle depth from alkaline melts. After the augite xenocrysts entered the magma, (001) lamellae first formed by spinodal decomposition at a $T_{min}$ of about 1,100 °C, and coarsened during very rapid transport to the surface; in a later phase, possibly on cooling, incipient (100) lamellae then formed.

## Introduction

Xenocrysts of mantle-related mineral phases (e.g. clinopyroxene, orthopyroxene, garnet, olivine) are found in alkali basalts worldwide. They probably crystallised from melts at variable depths and/or represent disaggregated peridotitic/pyroxenitic mantle nodules, and can provide important insights into related source(s).

The Hannuoba region (Hebei province, China) consists of a wide plateau of alkali basalts containing abundant mantle-derived mineral xenocrysts, sometimes forming up to 90% of the outcrop (Zhi et al. 1990). Song and Frey (1990) related the origin of the Hannuoba xenocrysts [mainly clinopyroxene (Cpx), garnet (Grt) and minor Fe–Ti oxides] to the crystallisation (and fractionation) from alkali basalts in the garnet stability field. The close association of mantle spinel–peridotite nodules with such alkali basalts also supports a mantle depth origin of the Cpx–Grt xenocrysts and their rapid ascent to the surface, providing important information on the subcontinental mantle.

The Hannuoba augite xenocrysts were studied by means of electron and X-ray diffraction techniques. X-ray single crystal diffraction evidenced the presence of exsolved augite and pigeonite in all the studied fragments. As exsolution microtextures depend to a great extent on physical conditions (e.g. temperature, pressure), they may allow the main development stages (e.g. from mantle depth towards the surface, cf. Putnis and McConnell 1980) to be traced. Various exsolution microtextures in pyroxenes are reported from both terrestrial and extraterrestrial bodies. Their differing microstructural textures are time and temperature dependent, and may be used to infer the thermal evolution of the host rocks (e.g. Nord et al. 1976).

This paper examines the significance of the exsolution microtextures present in the Hannuoba augitic xenocrysts, mainly as regards thermal and pressure conditions.

## Geological and petrographic outlines

Basaltic volcanism controlled by the Yanshang fault system occurs in the Hannuoba region, 10–20 km northwest of the town of Zhangjiankou city. According to their stratigraphy, palaeontology and geochronology, the Hannuoba basalts range in age from Miocene to

E. Brizi · S. Nazzareni (✉) · P. F. Zanazzi
Dipartimento di Scienze della Terra, Università di Perugia,
Piazza Università 1, I-06100 Perugia, Italy
E-mail: crystal1@unipg.it
Tel.: +39-75-5852611
Fax: +39-75-5852603

F. Princivalle
Dipartimento di Scienze della Terra, Università di Trieste,
Via Weiss 8, I-34127 Trieste, Italy

Editorial responsibility: V. Trommsdorff

Pliocene. On the CIPW normative basis, they range from basanites to quartz tholeiites. In addition, some basalt flows have compositional features intermediate between Ne- and Qz-normative basalts.

Alkaline lavas containing mantle xenoliths are generally classified by Feng et al. (1986) and Zhi et al. (1990) as alkali basalts. They are fine-grained, dark grey and massive, and enclose xenocrysts of clinopyroxene, alkali feldspar and a wide range of spinel-peridotitic mantle nodules. Vitrophyric to porphyritic alkali basalts have olivine, nepheline and smaller amounts of plagioclase phenocrysts set in a fine groundmass containing feldspars and glass. Grey to brownish-grey tholeiitic and transitional basalts (Zhi et al. 1990) are coarser in grain size, and are free of xenocrysts and peridotite nodules.

The clinopyroxene xenocrysts studied here come from Damaping village (Hannuoba region), where there is a large accumulation zone of spinel peridotite mantle nodules (up to 20 cm across) enclosed in alkali basalts. The latter also contain abundant clinopyroxene xenocrysts from centimetric to decimetric in size (Fig. 1). Song and Frey (1990) interpreted them as due to early partial melting stages of asthenospheric mantle, and the augite xenocrysts would be related to crystallisation of the alkali basalts. The composition and absence of zoning patterns, as well as the dimensions and presence of primary calcite in the augite xenocrysts, suggest deep mantle crystallisation. It should also be noted that the xenocrysts have sharp reaction rims (up to 2 mm across), mainly constituted of glass and/or radial olivine, suggesting rapid cooling and chemical disequilibrium with the host basalt.

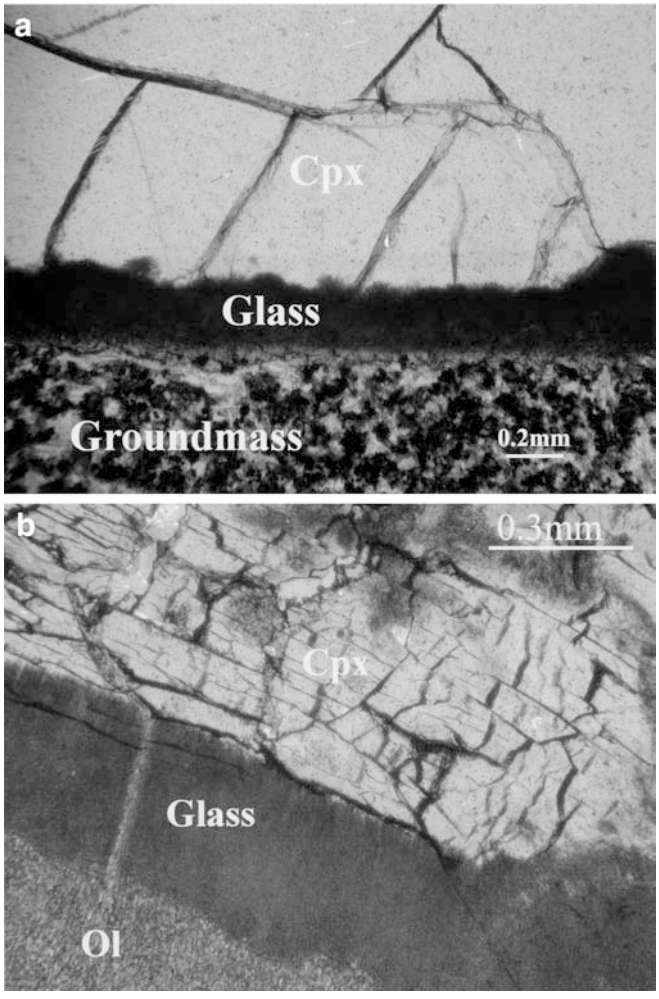


**Fig. 1** **a** C5 and **b** C10 augitic xenocrysts (parallel Nicols), showing sharp reaction rims of glass (C5) and radial olivine (C10)

## Experimental techniques

### TEM study

Transmission electron microscopy work was done according to the standard procedure described by Mellini (1989), using a TEM Philips 400T microscope operating at 100–120 kV (Electron Microscopy Centre, University of Perugia) and a JEOL JEM 2010 operating at 200 kV with a point-to-point resolution of 1.94 Å (Department of Earth Sciences, University of Siena).

TEM observations were performed on both crushed material and ion-thinned fragments, prepared following the technique described in Mellini (1989). Compositional data were obtained by a Link Energy Dispersive System (EDS) spectrometer, mounted on the TEM JEOL JEM 2010, from X-rays emitted by electron-transparent regions, using spot diameters of 250 and 100 down to 50 Å to analyse the exsolved phases, respectively. Semi-quantitative analyses were obtained following the Cliff–Lorimer approximation (Cliff and Lorimer 1975) using experimentally determined K-factors. Natural cordierite, phengite, kirschteinite, lizardite, pyroxene and sillimanite were used as standards.

### XRD study

Fragments of the same crystals used for TEM investigation were studied on a single-crystal four circle diffractometer XCALIBUR (Department of Earth Sciences, University of Perugia), equipped with a CCD (charge-coupled device) area detector. In our case, the advantage of working with the CCD detector technique is that the diffraction effects of more than one co-existent phase, to reveal the possible presence of exsolved phases, can be collected simultaneously and separately. Data collection was performed on single crystals of samples C5 and C10 in the same crystal-to-detector distance conditions (6.5 cm), but varying the theta range up to 55°, and omega and/or phi scans. Data from at least three-quarters to the whole limiting Ewald sphere were collected with monochromatised Mo radiation, and a reflection redundancy of about 1.8–5.3 was obtained.

The Ewald sphere image was visualised starting from data collection by the CrysAlis software package: exploring the reciprocal space, the various crystal orientations were inspected and the three lattice vectors for the augitic and pigeonitic phases were subsequently chosen. Structural refinements were carried out on both pigeonite lamellae and augite matrix (Brizi et al. 2002). The CrysAlis software also provides reciprocal lattice plane (precession-like) images with very sensitive resolution. The bulk chemical composition of the xenocrysts was measured using a Cameca/Camebax electron microprobe with a WDS system (EMPA) operating with a 1-$\mu$m beam at 15 kV and 20 nA, and counting times of 20 s for peak and background, as reported by Brizi et al. (2000). Up to ten spot analyses were averaged to obtain the mean composition of the crystals.

### Crystal chemistry details

Single-crystal fragments from C5 and C10 augite xenocrysts were carefully selected in order to avoid even feeble optical inhomoge-

neities and inclusions. In spite of their sharp extinction under the polarising microscope, they revealed systematic X-ray extinctions typical of a primitive lattice ($h+k=2n+1$), in contrast with $C2/c$ space group rules, suggesting the occurrence of submicroscopic fine-scale exsolution microtextures.

EMP analyses showed the studied crystal fragments to be chemically homogeneous; the average compositions for the exsolved phases, analysed by EDS-TEM, are listed in Table 1. In sample C5, the (001) lamellae were more difficult to analyse, the high Ca content indicating contamination from the matrix. Thus, we report the mean of five points analyses and one single analysis, presenting the lowest Ca content, which is close to the value of the (001) lamellae composition of sample C10. According to Lindsley (1983), the minimum crystallisation temperature for both sub-calcic samples is between 1,200 and 1,100 °C.

From a structural point of view, the studied augitic xenocrysts have cell and site volumes compatible with crystallisation from alkali basalts in mantle depth conditions (Fig. 2; Dal Negro et al. 1989). In spite of their similar cell volume, these augitic xenocrysts have tetrahedral site volumes greater than those of C2/c pyroxenes belonging to the associated fertile-depleted spinel peridotite mantle nodules (Princivalle et al. 1998), which underwent variable degrees of basalt extraction. This is due to the high content of Al in tetrahedral site, which is another typical characteristic of clinopyroxene crystallised from alkaline melts at mantle depth, as reported by Dal Negro et al. (1989) for high-pressure clinopyroxene megacrysts from Victoria (Australia).

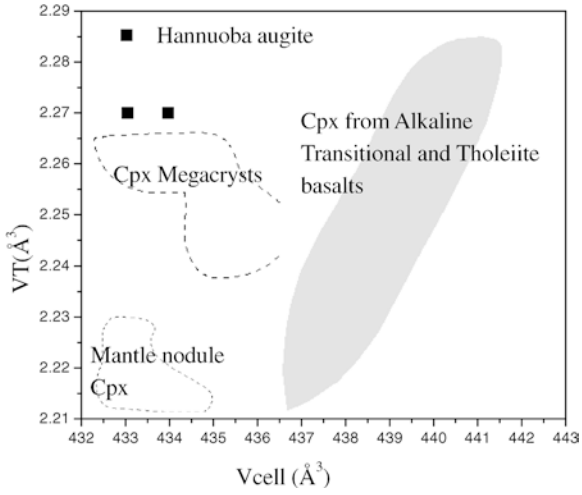


**Fig. 2** Tetrahedral volume vs cell volume for samples C5 and C10. *Grey field* Cpx from alkaline, transitional and tholeiitic basalts; *dashed fields: 1* Cpx megacrysts from Victoria; *2* Cpx from spinel peridotite nodules (Dal Negro et al. 1989)

## Microtextural aspects

Both samples C5 and C10 show exsolution microtextures: the sub-calcic augite host exsolved into augite and coherent (001) and (100) lamellae of pigeonite. The (001) lamellae are diffuse and vary in thickness between 100 to 300 Å in samples C10 and C5, respectively; the (100) lamellae are incipient and have thickness lower than 70 Å. Representative images of the pigeonite–augite exsolution microtextures are shown in Fig. 3. A high-

**Table 1** Average analyses of C5 and C10 pyroxenes: clinopyroxene bulk compositions analysed by WDS-EMP, (001) pigeonite lamellae and augite matrix compositions by EDS-TEM. Na, Ti, Cr and Mn contents in exsolved phases were not determined. Oxides are expressed in wt%, and cations in atoms per formula unit. The asterisk on (001) pigeonite lamellae, indicates the composition from one-spot analysis (see text for explanation)

| China | C5 | | | | C10 | | |
|---|---|---|---|---|---|---|---|
| | Clinopyroxene bulk EMPA | (001) Pigeonite lamellae EDS-TEM | (001) Pigeonite lamellae* EDS-TEM | Augite matrix EDS-TEM | Clinopyroxene bulk EMPA | (001) Pigeonite lamellae EDS-TEM | Augite matrix EDS-TEM |
| $SiO_2$ | 50.9 (5) | 54.1 (4) | 54.94 | 50.7 (5) | 51.2 (4) | 54.2 (4) | 49.9 (4) |
| $Al_2O_3$ | 8.46 (4) | 4.78 (15) | 4.89 | 8.34 (12) | 8.41 (8) | 4.25 (10) | 8.61 (9) |
| TiO | 0.66 (10) | n.d. | n.d. | n.d. | 0.61 (3) | n.d. | n.d. |
| $Cr_2O_3$ | 0.06 (3) | n.d. | n.d. | n.d. | 0.07 (2) | n.d. | n.d. |
| MgO | 16.67 (18) | 20.66 (17) | 22.34 | 14.34 (16) | 16.43 (13) | 20.95 (18) | 14.93 (15) |
| FeO | 7.56 (5) | 12.3 (6) | 12.44 | 7.97 (9) | 7.6 (2) | 14.8 (2) | 8.2 (2) |
| MnO | 0.13 (8) | n.d. | n.d. | n.d. | 0.15 (7) | n.d. | n.d. |
| CaO | 14.88 (5) | 8.10 (18) | 5.38 | 18.65 (17) | 14.98 (9) | 5.88 (15) | 18.36 (14) |
| NaO | 1.45 (4) | n.d. | n.d. | n.d. | 1.45 (5) | n.d. | n.d. |
| Total | 100.77 | 100 | 100 | 100 | 100.9 | 100 | 100 |
| Si | 1.826 (10) | 1.95 (2) | 1.96 | 1.86 (3) | 1.843 (5) | 1.960 (8) | 1.830 (7) |
| Al | 0.358 (5) | 0.20 (2) | 0.21 | 0.36 (2) | 0.357 (3) | 0.180 (5) | 0.370 (5) |
| Ti | 0.018 (1) | n.d. | n.d. | n.d. | 0.017 (1) | n.d. | n.d. |
| Cr | 0.002 (1) | n.d. | n.d. | n.d. | 0.002 (1) | n.d. | n.d. |
| Mg | 0.892 (2) | 1.11 (7) | 1.19 | 0.78 (7) | 0.881 (6) | 1.135 (8) | 0.815 (9) |
| $Fe^{2+}$ | 0.174 (12) | 0.37 (3) | 0.37 | 0.24 (5) | 0.230 (6) | 0.450 (9) | 0.250 (7) |
| $Fe^{3+}$ | 0.054 (18) | n.d. | n.d. | n.d. | – | n.d. | n.d. |
| Mn | 0.004 (2) | n.d. | n.d. | n.d. | 0.004 (2) | n.d. | n.d. |
| Ca | 0.572 (2) | 0.31 (8) | 0.21 | 0.73 (7) | 0.577 (4) | 0.230 (5) | 0.720 (6) |
| Na | 0.101 (3) | n.d. | n.d. | n.d. | 0.101 (3) | n.d. | n.d. |
| Wo | 34 | 17 | 12 | 42 | 34 | 13 | 40 |
| En | 53 | 62 | 67 | 44 | 52 | 62 | 46 |
| Fs | 13 | 21 | 21 | 14 | 14 | 25 | 14 |

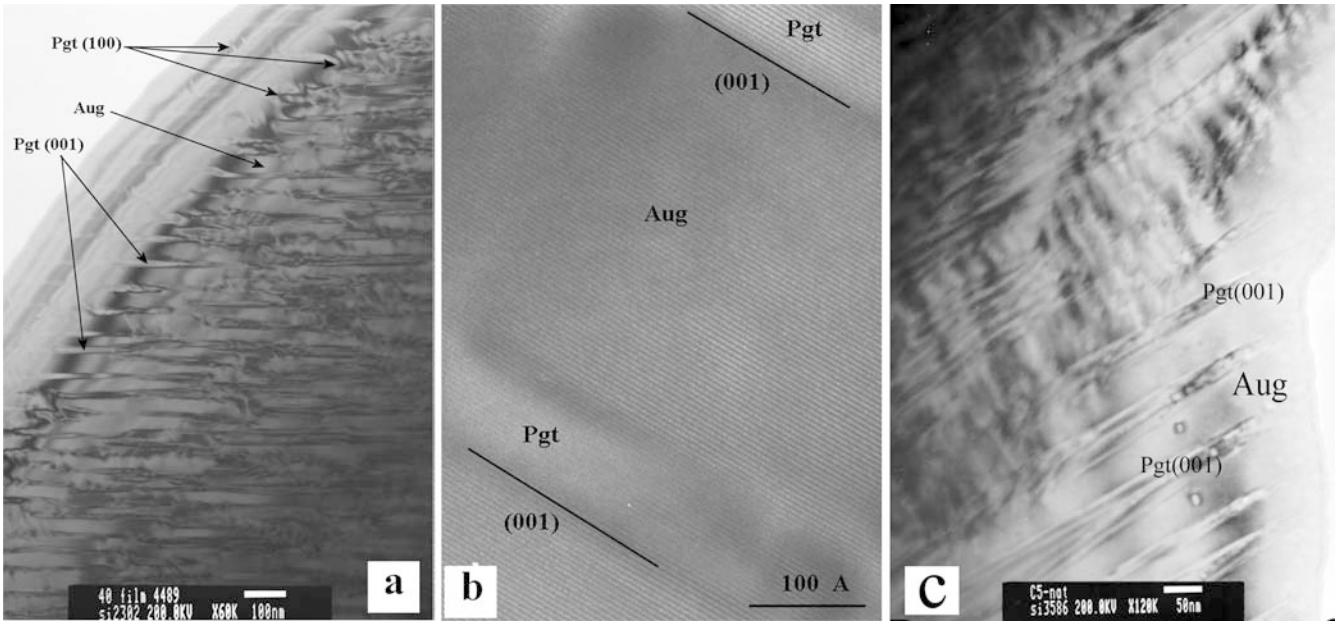


**Fig. 3** TEM images of exsolution textures. *a* sample C10, bright field; *b* high-resolution image of (001) contact plane between pigeonite and augite in sample C10; *c* sample C5, bright field

resolution image shows the interface between augite and pigeonite (Fig. 3b). The branching feature of the lamellae suggests that the exsolution reaction is due to a spinodal decomposition mechanism.

The electron diffraction patterns (Fig. 4) observed along the [1 $\bar{3}$ 0] direction for C10 and for C5, reveals well split spots along the [0 0 1]* direction. This geometry suggests that pigeonite lamellae occur on the (001) plane. Some weak streaking along *a** may be due to the (100) lamellae. As shown by TEM images, the (001) lamellae are coarser than the (100) ones due to the different elastic strain energy in the two orientations.

Semi-quantitative analyses of the exsolved phases (Table 1) define a minimum exsolution temperature of around 1,100 °C (Lindsley 1983).

## Structural aspects

Data collected by the X-ray CCD area detector clearly show the presence of two exsolved phases, as also shown by TEM: a more abundant phase with augite $C2/c$ structure (about 80 vol%), and a smaller one (20 vol%) with $P2_1/c$ pigeonite structure. These two monoclinic lattices relate through $a(\text{Aug}) = a(\text{Pgt})$, $b(\text{Aug}) = b(\text{Pgt})$, $c(\text{Aug}) \neq c(\text{Pgt})$ and $\Delta\beta \cong 2.0°$ (Table 2), suggesting that the pigeonitic phase mainly occurs with complete coherency along *c**. Coherency along *c** and the augite–pigeonite lattice relations confirm the (001) orientation of the pigeonite lamellae, as testified by TEM images. The same structural configuration occurs in the precession-like image obtained from data for the ($h$ 1 $l$) plane (Fig. 5). Both samples C10 and C5 show the splitting of ($h+k$) even reflections (*a*-class) and ($h+k$) odd reflections (*b*-class), both due to the primitive pigeonite lattice. It should also be noted that the *a*-class reflections

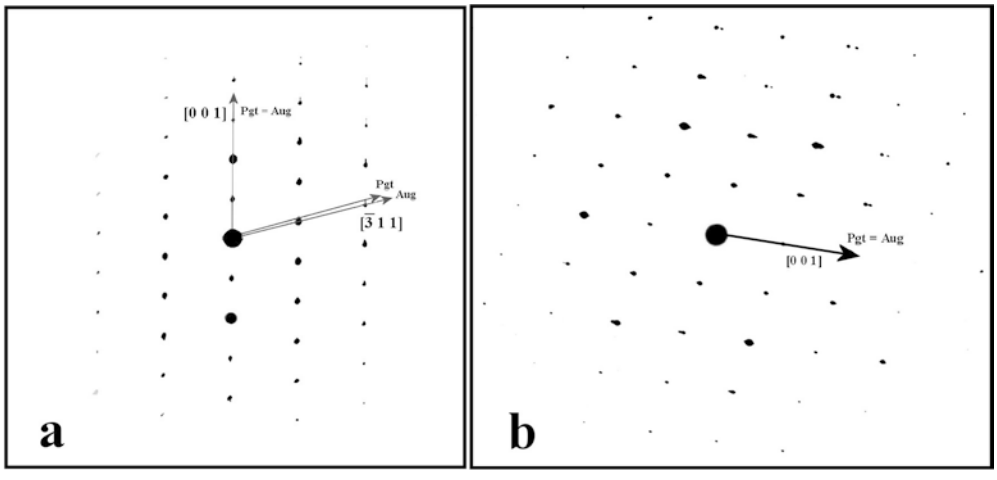


**Fig. 4** Electron diffraction pattern, showing slightly rotated pigeonite and augite lattices in samples **a** C10 and **b** C5

**Table 2** Lattice parameters (in Å) and cell and tetrahedral volumes (in $Å^3$) of augite and pigeonite exsolved pairs for C10 and C5 pyroxenes. C5-1 and C5-2 refer to two CCD-XRD data collections

| China | C10 (001) Pigeonite | C10 Augite | C5-1 (001) Pigeonite | C5-1 Augite | C5-2 (001) Pigeonite | C5-2 Augite |
|---|---|---|---|---|---|---|
| *a* | 9.689 (2) | 9.691 (1) | 9.698 (3) | 9.682 (1) | 9.687 (2) | 9.678 (1) |
| *b* | 8.847 (2) | 8.852 (1) | 8.854 (2) | 8.857 (1) | 8.846 (3) | 8.847 (1) |
| *c* | 5.200 (1) | 5.278 (1) | 5.210 (2) | 5.269 (1) | 5.189 (2) | 5.275 (10) |
| *β* | 108.55 (2) | 106.56 (1) | 108.35 (3) | 106.64 (2) | 108.47 (3) | 106.49 (1) |
| Vcell | 422.57 | 433.97 | 424.62 | 432.91 | 421.75 | 433.05 |
| VT | – | 2.265 (3) | – | – | – | 2.266 (2) |

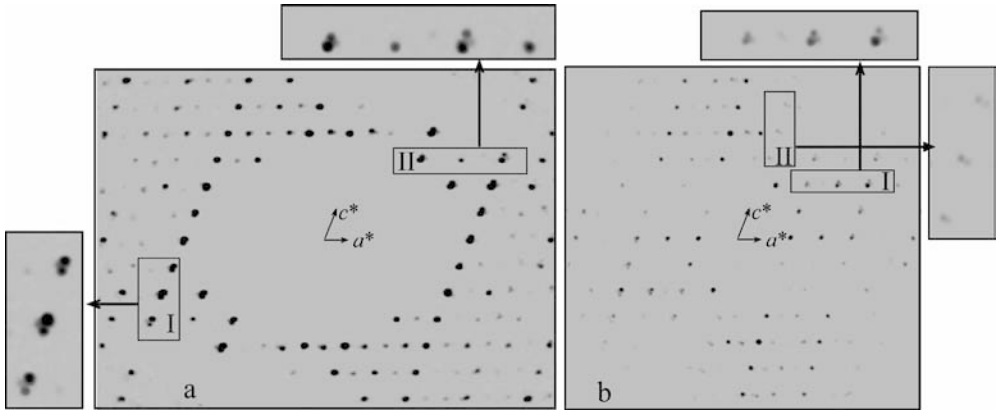


**Fig. 5** CCD-RX precession-like image of (*h* 1 *l*) plane. *a* Sample C10; *insets* zoom of $(\bar{7}\ 1\ \bar{l})$ (I) and (*h* 1 3 ) rows (II), showing splitting of $(h+k=2n)$ reflections of pigeonite phase along both *a** and *c** directions. ***b*** Sample C5; *insets* zoom on (*h* 1 2) row (I) with split pigeonite spots, and (0 1 *l*) row due only to pigeonite lamellae

split not only along *c** [due to the (001) lamellae], but also along *a** [due to the incipient (100) lamellae] in both samples.

The orientation matrix for *C*2/c augite and (001) pigeonite lamellae were calculated with the CrysAlis software package (Oxford diffraction); thus, allowing measurement of the lattice parameters of the exsolved and matrix phases, as listed in Table 2.

## Discussion

The systematic extinctions, violating *C*2/*c* space group rules, shown by the Hannuoba xenocrysts are satisfactorily explained (TEM, CCD XRD) by the presence of exsolution microstructures within the augite crystals. The exsolutions are given by (1) (001) lamellae bidimensionally infinite and varying in thickness from 100 to 300 Å; (2) by an incipient (100) set, with thickness lower than 70 Å. Samples C5 and C10 have similar bulk and exsolved phase composition (Table 1), but the pigeonite lamellae differ in thickness, suggesting different time and/or thermal conditions of growth. This was to be expected, considering that the augite xenocrysts are in thermal and chemical disequilibrium with the host magma, as shown by petrographical evidence. In addition, the presence of spinel-peridotitic mantle nodules in the same host alkali basalt supports the hypothesis that the augite xenocrysts crystallised in mantle depth conditions.

In the augite–pigeonite exsolution process, the growth of exsolved phases is maximum when the interfacial strain is minimum. Strain energy is very important because exsolution lamellae tend to form along planes normal to elastically 'soft' directions (Buseck et al. 1980). For augite–pigeonite lattices, there are two directions along which interfacial energy is minimum, i.e. (001) and (100) planes. The strain energy associated with (001) plane is about twice as high as that of (100) plane (Buseck et al. 1980).

Referring to the (001) coherent solvus and coherent spinodal, calculated by McCallister and Nord (1981) for pigeonite exsolution in augite at 1 atm, a clinopyroxene with Ca/(Ca + Mg) of about 0.4 (i.e. the clinopyroxene composition of samples C5 and C10) falls on the coherent solvus at 1,000 °C, whereas the inferred exsolution temperature for (001) lamellae is 1,100 °C. However, it should be recalled that, according to Lindsley (1980), a pressure increase widens the metastable pigeonite–diopside solvus, indicating that the (001) pigeonite lamellae may have exsolved at high pressure, as supported by petrological (i.e. peridotitic mantle nodules and closely associated augite xenocrysts) and structural data (i.e. cell and site volumes).

In our case, there was time and energy to exsolve coherent (001) lamellae of pigeonite at an exsolution temperature down to 1,100 °C. Spinodal decomposition may have started somewhere between the heterogeneous mantle and the surface when the augitic xenocrysts entered alkaline lava or during their ascent to the surface. In any case, they underwent a decrease in temperature and/or pressure in a very short time.

The absence of anti-phase domains (APD) in the pigeonitic lamellae suggests that pigeonite enucleated below the high-low pigeonite transition temperature, as APD's are believed to form during phase transition.

Thus, the (001) lamellae may have formed in space group $C2/c$ or $P2_1/c$, depending on the (P,T) conditions of exsolution. Using the relation suggested by Arlt et al. (2000) between the average cation size on M2 site and the HT (high temperature)-transition temperature, our sub-calcic augites underwent transition at about 1,100 °C, with a minimum of 850 °C; for a composition $En_{47}Fs_{43}Wo_{10}$, the HT-transition temperature has also been reported to be around 875–925 °C at 1 atm (Camara et al. 2002). Applying the average slope boundary for the $P2_1/c$-HT $C2/c$ transition suggested by Arlt et al. (2000), the (001) lamellae formed in space group $C2/c$ only up to about 2 GPa.

With decreasing temperature, the pigeonite $\beta$ angle decreases much more than the augite $\beta$ angle with temperature. Thus, the pigeonite, constrained in the augite host, adjusts this angle variation forming stacking faults on (100) planes. These faults generate partial dislocation where the strain is locally concentrated; so that the dislocation planes may become suitable sites for the further development of lamellae.

When the xenocrysts entered the alkaline basalts, a new thermal regime was achieved, and spinodal decomposition started, forming and coarsening a first set of exsolution lamellae along (001) plane. A new set of lamellae along the (100) plane formed later because the interfacial energy term for the (001) lamellae became more and more important, and in order to lower the total free energy, (100) lamella nucleation at the end of the stacking faults was enhanced.

The Hannuoba alkaline magmas may have enclosed the augitic xenocrysts from the wall conduit at various depths, and they rapidly reached the surface, having a high ascent rate. Applying the coarsening law proposed by Grove (1982), around 43 h are required to coarsen the (001) lamellae in sample C5 and around 38 h in sample C10. Assuming an ascent rate of 50 cm/s (Spera 1984) and a magma depth of about 60 km, the magma could have reached the surface in about 30 h.

The exsolution process of (001) lamellae may have started at depth, before the augitic xenocrysts entered the magma, and was completed during ascent; alternatively, it may have developed during the ascent and was then completed on cooling. During the eruption, the (100) new pigeonite lamellae began to form, but cooling was too fast to allow their coarsening.

## Conclusions

The Hannuoba augite xenocrysts and associated spinel peridotite nodules sampled by alkali basalts indicate great compositional heterogeneity of the subcontinental lithospheric mantle. The augite xenocrysts, which crystallised at high pressure, are optically homogeneous but are characterised by two sets of pigeonite exsolution lamellae revealing different thermal conditions. The first set, oriented (001) and 100–300 Å thick, formed by spinodal decomposition during very rapid transport to the surface, starting at depth at a minimum temperature of about 1,100 °C. The second set, oriented (100) and $< 70$ Å thick, is incipient and formed after the first one, possibly on cooling after eruption.

**Acknowledgements** The authors are indebted to E.M. Piccirillo for a critical review of the text, and to G.C. Capitani for help during the TEM study. M. Mellini and an anonymous referee improved the manuscript. F. Princivalle would like to thank the Chinese Academy of Science for funding his visit to China in 1998, and J. Feng and Y. Wanming for their precious support and help given in field sampling. The authors also acknowledge the financial support of MURST grants (COFIN '01, project 'Transformations, reactions, ordering in minerals') to F. Princivalle and P.F. Zanazzi. The English text was revised by Gabriel Walton.

## References

Arlt T, Kunz M, Stolz J, Armbruster T, Angel R (2000) P–T–X data on $P2_1/c$-clinopyroxenes and their displacive phase transition. Contrib Mineral Petrol 138:35–45

Brizi E, Molin G, Zanazzi PF (2000) Experimental study of intracrystalline $Fe^{2+}$–Mg exchange in three augite crystals: effect of composition on geothermometric calibration. Am Mineral 85:1375–1382

Brizi E, Nazzareni S, Princivalle F, Zanazzi PF (2002) Microtextural and structural aspects of augitic megacrystals from alkali basalts of Hannuoba region (China). Proc 18th IMA Conf Program with Abstract, pp 94–95

Buseck PR, Nord GL Jr, Veblen DR (1980) Subsolidus phenomena in pyroxenes. In: Prewitt CT (ed) Reviews in mineralogy, vol 7. Pyroxene, Mineral Soc Am, pp 117–180

Camara F, Carpenter MA, Domeneghetti MC, Tazzoli V (2002) Non-convergent ordering and displacive phase transition in pigeonite: in situ HT XDR study. Phys Chem Mineral 29:331–340

Cliff G, Lorimer GW (1975) The quantitative analysis of thin specimens. J Microsc 103:203–207

Dal Negro A, Manoli S, Secco L, Piccirillo EM (1989) Megacrystic clinopyroxenes from Victoria (Australia): crystal chemical comparisons of pyroxenes from high and low pressure regimes. Eur J Mineral 1:105–121

Feng J, Xie M, Zheng H (1986) Geochemical characteristics of rare earth elements in Hannuoba basalts (in Chinese, with English abstract). Bull Hebei Geol Coll 9:217–232

Grove T (1982) Use of exsolution lamellae in lunar clinopyroxenes as cooling rate speedometers: an experimental calibration. Am Mineral 67:251–268

Lindsley DH (1980) Phase equilibria of pyroxenes at pressures $>1$ atmosphere. In: Prewitt CT (ed) Reviews in mineralogy, vol 7. Pyroxene. Mineral Soc Am, pp 289–308

Lindsley DH (1983) Pyroxene thermometry. Am Mineral 68:477–493

McCallister RH, Nord GL Jr (1981) Subcalcic diopsides from kimberlites: chemistry, exsolution microstructures, and thermal history. Contrib Mineral Petrol 78:118–125

Mellini M (1989) High resolution transmission electron microscopy and geology. In: Advances in electronics and electron physics. Academic Press, New York, pp 281–326

Nord GL, Heuer AH, Lalli JL (1976) Pigeonite exsolution from augite. In: Wenk HR (ed) Electron microscopy in mineralogy. Springer, Berlin Heidelberg New York, pp 220–227

Princivalle F, Wanming Y, Feng J, Comin-Chiaramonti P (1998) Crystal chemistry of the constituent phases of a spinel peridotite xenolith from Hannuoba region (China). Mineral Petrogr Acta XLI:35–42

Putnis A, McConnell JDC (1980) Principles of mineral behaviour. Blackwell, Oxford

Song Y, Frey FA (1990) Geochemistry of peridotite xenoliths in basalt from Hannuoba, Eastern China: implications for subcontinental mantle heterogeneity. Geochem Cosmochim Acta 53:97–113

Spera FJ (1984) Carbon dioxide in petrogenesis. III Role of volatiles in the ascent of alkaline magma with special reference to xenolith-bearing mafic lavas. Contrib Mineral Petrol 88:217–232

Zhi Z, Song Y, Frey FA, Feng J, Zhai M (1990) Geochemistry of Hannuoba basalts, Eastern China: constraints on the origin of continental alkali and tholeiitic basalt. Chem Geol 88:1–33